



**HAL**  
open science

## Extended $p_{3/2}$ Neutron Orbital and the $N = 32$ Shell Closure in $^{52}\text{Ca}$

M. Enciu, H.N. Liu, A. Obertelli, P. Doornenbal, F. Nowacki, K. Ogata, A. Poves, K. Yoshida, N.L. Achouri, H. Baba, et al.

► **To cite this version:**

M. Enciu, H.N. Liu, A. Obertelli, P. Doornenbal, F. Nowacki, et al.. Extended  $p_{3/2}$  Neutron Orbital and the  $N = 32$  Shell Closure in  $^{52}\text{Ca}$ . *Physical Review Letters*, 2022, 129 (26), pp.262501. 10.1103/PhysRevLett.129.262501 . hal-03909049

**HAL Id: hal-03909049**

**<https://hal.science/hal-03909049>**

Submitted on 20 Nov 2023

**HAL** is a multi-disciplinary open access archive for the deposit and dissemination of scientific research documents, whether they are published or not. The documents may come from teaching and research institutions in France or abroad, or from public or private research centers.

L'archive ouverte pluridisciplinaire **HAL**, est destinée au dépôt et à la diffusion de documents scientifiques de niveau recherche, publiés ou non, émanant des établissements d'enseignement et de recherche français ou étrangers, des laboratoires publics ou privés.



Distributed under a Creative Commons Attribution 4.0 International License

**Extended  $p_{3/2}$  Neutron Orbital and the  $N = 32$  Shell Closure in  $^{52}\text{Ca}$** 

M. Enciu<sup>1,\*</sup>, H. N. Liu<sup>1,2,3,†</sup>, A. Obertelli<sup>1,4,5</sup>, P. Doornenbal<sup>5</sup>, F. Nowacki<sup>6</sup>, K. Ogata<sup>7,8</sup>, A. Poves<sup>9</sup>, K. Yoshida<sup>10</sup>, N. L. Achouri<sup>11</sup>, H. Baba<sup>5</sup>, F. Browne<sup>5</sup>, D. Calvet<sup>4</sup>, F. Château<sup>4</sup>, S. Chen<sup>12,5,13</sup>, N. Chiga<sup>5</sup>, A. Corsi<sup>4</sup>, M. L. Cortés<sup>5</sup>, A. Delbart<sup>4</sup>, J.-M. Gheller<sup>4</sup>, A. Giganon<sup>4</sup>, A. Gillibert<sup>4</sup>, C. Hilaire<sup>4</sup>, T. Isobe<sup>5</sup>, T. Kobayashi<sup>14</sup>, Y. Kubota<sup>5,15</sup>, V. Lapoux<sup>4</sup>, T. Motobayashi<sup>5</sup>, I. Murray<sup>16,5</sup>, H. Otsu<sup>5</sup>, V. Panin<sup>5</sup>, N. Paul<sup>4,17</sup>, W. Rodriguez<sup>5,18,19</sup>, H. Sakurai<sup>5,20</sup>, M. Sasano<sup>5</sup>, D. Steppenbeck<sup>5</sup>, L. Stuhl<sup>15,21,22</sup>, Y. L. Sun<sup>4,1</sup>, Y. Togano<sup>23,5</sup>, T. Uesaka<sup>5</sup>, K. Wimmer<sup>20,5</sup>, K. Yoneda<sup>5</sup>, O. Aktas<sup>3</sup>, T. Aumann<sup>1,24</sup>, L. X. Chung<sup>25</sup>, F. Flavigny<sup>16,11</sup>, S. Franchoo<sup>16</sup>, I. Gasparic<sup>26,1,5</sup>, R.-B. Gerst<sup>27</sup>, J. Gibelin<sup>11</sup>, K. I. Hahn<sup>28,22</sup>, D. Kim<sup>28,5,22</sup>, Y. Kondo<sup>29</sup>, P. Koseoglou<sup>1,24</sup>, J. Lee<sup>12</sup>, C. Lehr<sup>1</sup>, P. J. Li<sup>12</sup>, B. D. Linh<sup>25</sup>, T. Lokotko<sup>12</sup>, M. MacCormick<sup>16</sup>, K. Moschner<sup>27</sup>, T. Nakamura<sup>29</sup>, S. Y. Park<sup>28,22</sup>, D. Rossi<sup>1</sup>, E. Sahin<sup>30</sup>, P.-A. Söderström<sup>1</sup>, D. Sohler<sup>21</sup>, S. Takeuchi<sup>29</sup>, H. Toernqvist<sup>1,24</sup>, V. Vaquero<sup>31</sup>, V. Wagner<sup>1</sup>, S. Wang<sup>32</sup>, V. Werner<sup>1,33</sup>, X. Xu<sup>12</sup>, H. Yamada<sup>29</sup>, D. Yan<sup>32</sup>, Z. Yang<sup>5</sup>, M. Yasuda<sup>29</sup> and L. Zanetti<sup>1</sup>

<sup>1</sup>*Institut für Kernphysik, Technische Universität Darmstadt, 64289 Darmstadt, Germany*

<sup>2</sup>*Key Laboratory of Beam Technology of Ministry of Education, College of Nuclear Science and Technology, Beijing Normal University, Beijing 100875, China*

<sup>3</sup>*Department of Physics, Royal Institute of Technology, SE-10691 Stockholm, Sweden*

<sup>4</sup>*IRFU, CEA, Université Paris-Saclay, F-91191 Gif-sur-Yvette, France*

<sup>5</sup>*RIKEN Nishina Center, 2-1 Hirosawa, Wako, Saitama 351-0198, Japan*

<sup>6</sup>*Université de Strasbourg, CNRS, IPHC UMR 7178, F-67000 Strasbourg, France*

<sup>7</sup>*Department of Physics, Kyushu University, Fukuoka 819-0395, Japan*

<sup>8</sup>*Research Center for Nuclear Physics (RCNP), Osaka University, Ibaraki 567-0047, Japan*

<sup>9</sup>*Departamento de Física Teórica and IFT UAM-CSIC, Universidad Autónoma de Madrid, Spain*

<sup>10</sup>*Advanced Science Research Center, Japan Atomic Energy Agency, Tokai, Ibaraki 319-1195, Japan*

<sup>11</sup>*LPC Caen, Normandie Université, ENSICAEN, UNICAEN, CNRS/IN2P3, F-14000 Caen, France*

<sup>12</sup>*Department of Physics, The University of Hong Kong, Pokfulam, Hong Kong*

<sup>13</sup>*State Key Laboratory of Nuclear Physics and Technology, Peking University, Beijing 100871, China*

<sup>14</sup>*Department of Physics, Tohoku University, Sendai 980-8578, Japan*

<sup>15</sup>*Center for Nuclear Study, University of Tokyo, RIKEN campus, Wako, Saitama 351-0198, Japan*

<sup>16</sup>*Université Paris-Saclay, CNRS/IN2P3, IJCLab, F-91405 Orsay cedex, France*

<sup>17</sup>*Laboratoire Kastler Brossel, Sorbonne Université, CNRS, ENS, PSL Research University, Collège de France, Case 74, 4 Place Jussieu, 75005 Paris, France*

<sup>18</sup>*Pontificia Universidad Javeriana, Facultad de Ciencias, Departamento de Física, Bogotá, Colombia*

<sup>19</sup>*Universidad Nacional de Colombia, Sede Bogotá, Facultad de Ciencias, Departamento de Física, Bogotá 111321, Colombia*

<sup>20</sup>*Department of Physics, University of Tokyo, 7-3-1 Hongo, Bunkyo, Tokyo 113-0033, Japan*

<sup>21</sup>*Institute for Nuclear Research, Atomki, P.O. Box 51, Debrecen H-4001, Hungary*

<sup>22</sup>*Institute for Basic Science, Daejeon 34126, Korea*

<sup>23</sup>*Department of Physics, Rikkyo University, 3-34-1 Nishi-Ikebukuro, Toshima, Tokyo 172-8501, Japan*

<sup>24</sup>*GSI Helmholtzzentrum für Schwerionenforschung GmbH, Planckstrasse 1, 64291 Darmstadt, Germany*

<sup>25</sup>*Institute for Nuclear Science & Technology, VINATOM, 179 Hoang Quoc Viet, Cau Giay, Hanoi, Vietnam*

<sup>26</sup>*Ruđer Bošković Institute, Bijenička cesta 54, 10000 Zagreb, Croatia*

<sup>27</sup>*Institut für Kernphysik, Universität zu Köln, D-50937 Cologne, Germany*

<sup>28</sup>*Ewha Womans University, Seoul 03760, Korea*

<sup>29</sup>*Department of Physics, Tokyo Institute of Technology, 2-12-1 O-Okayama, Meguro, Tokyo, 152-8551, Japan*

<sup>30</sup>*Department of Physics, University of Oslo, N-0316 Oslo, Norway*

<sup>31</sup>*Instituto de Estructura de la Materia, CSIC, E-28006 Madrid, Spain*

<sup>32</sup>*Institute of Modern Physics, Chinese Academy of Sciences, Lanzhou 730000, China*

<sup>33</sup>*Helmholtz Forschungsakademie Hessen für FAIR (HFHF), GSI Helmholtzzentrum für Schwerionenforschung, Campus Darmstadt, 64289 Darmstadt, Germany*



(Received 9 August 2022; revised 24 October 2022; accepted 23 November 2022; published 20 December 2022)

The one-neutron knockout from  $^{52}\text{Ca}$  in inverse kinematics onto a proton target was performed at  $\sim 230$  MeV/nucleon combined with prompt  $\gamma$  spectroscopy. Exclusive quasifree scattering cross sections to bound states in  $^{51}\text{Ca}$  and the momentum distributions corresponding to the removal of  $1f_{7/2}$  and  $2p_{3/2}$  neutrons were measured. The cross sections, interpreted within the distorted-wave impulse approximation reaction framework, are consistent with a shell closure at the neutron number  $N = 32$ , found as strong as at  $N = 28$  and  $N = 34$  in Ca isotopes from the same observables. The analysis of the momentum distributions leads to a difference of the root-mean-square radii of the neutron  $1f_{7/2}$  and  $2p_{3/2}$  orbitals of 0.61(23) fm, in agreement with the modified-shell-model prediction of 0.7 fm suggesting that the large root-mean-square radius of the  $2p_{3/2}$  orbital in neutron-rich Ca isotopes is responsible for the unexpected linear increase of the charge radius with the neutron number.

DOI: [10.1103/PhysRevLett.129.262501](https://doi.org/10.1103/PhysRevLett.129.262501)

Atomic nuclei can be described as neutrons and protons bound in a self-induced attractive mean field [1]. In the shell-model picture, they occupy discrete energy levels, grouped into shells, while interacting with each other via nuclear residual interactions. Particularly stable configurations appear for full shells, associated to the so-called magic numbers of nucleons. The relative energies of single-particle orbitals are dynamic over the nuclear chart, driven by the monopole part of the residual interaction [2,3]. Far from stability the shell closures can disappear or weaken, e.g., at the neutron numbers  $N = 8, 20$ , and  $28$  [4–8], and new magic numbers can emerge. In the neutron-rich  $pf$ -shell nuclei, new shell closures at  $N = 32$  and  $34$  were revealed, corresponding to the filling of the  $2p_{1/2}$  and  $2p_{3/2}$  neutron orbitals, respectively. The  $N = 32$  shell closure in neutron-rich nuclei was claimed from a series of observations relying on first  $2^+$  excitation-energy [9–14], transition-probability [15,16], and mass measurements [17–20], correspondingly the  $N = 34$  shell closure from  $E(2^+)$  [21,22], mass [23], and neutron knockout cross-section [24] measurements. On the other hand, recent measurements along the Ca and K isotopic chains reveal an increase of the charge radii with a slope larger than expected from  $N = 28$  to  $N = 32$  and  $33$ , respectively, and with no local minimum or inflection at  $N = 32$ , which is usually considered as a sign of a neutron shell closure [25–27]. This observation, not quantitatively reproduced by microscopic theories, was interpreted as challenging the doubly closed-shell character of  $^{52}\text{Ca}$ . An erosion of the proton shell closure is not supported by spectroscopic experiments [28,29], while the connection between charge radii evolution and the strength of a neutron shell closure has been recently questioned [30]. As an alternative interpretation, an effective increase in size of shell-model valence  $p$ -wave neutron orbitals influencing the proton radial extension has been proposed to reproduce the observed increase of charge radii of Ca isotopes, while maintaining the doubly magic character of  $^{52}\text{Ca}$  [31]. A sizable difference of 0.7 fm was predicted between the root-mean-square (rms) radius of the  $2p_{3/2}$  and the  $1f_{7/2}$  neutron orbitals, in qualitative agreement with the matter radius trend of  $^{49-51}\text{Ca}$  isotopes extracted from interaction cross sections [32].

In this Letter, we address the neutron shell closure of  $^{52}\text{Ca}$  from direct neutron knockout ( $p, pn$ ) and we provide a first determination of the spatial extension of the  $1f_{7/2}$  and  $2p_{3/2}$  neutron orbitals.

The experiment was performed at the Radioactive Isotope Beam Factory of RIKEN, operated jointly by the RIKEN Nishina Center and the Center for Nuclear Study, University of Tokyo. A 240-pnA  $^{70}\text{Zn}$  primary beam at 345 MeV/nucleon impinged on a 10-mm-thick Be target for the production of the secondary cocktail beam. The beam-particle identification was done event by event using the BigRIPS separator [33] via magnetic-rigidity ( $B\rho$ ), energy-loss ( $\Delta E$ ), and time-of-flight (TOF) measurements [34]. The  $^{52}\text{Ca}$  particles were produced with a mean intensity of 4.4 particles per second (2.3% purity).

The ( $p, pn$ ) reaction was measured at the SAMURAI setup [35] using MINOS [36] and DALI2<sup>+</sup> [37]. MINOS was composed of a 151(1) mm liquid-hydrogen target with a density of 73 mg/cm<sup>3</sup> surrounded by a 300-mm-long time projection chamber allowing a reaction vertex reconstruction with a resolution of 5 mm full-width-at-half-maximum (FWHM) [38]. The prompt  $\gamma$  rays from the deexcitation of the  $^{51}\text{Ca}$  fragments were measured with DALI2<sup>+</sup>, a high-efficiency array of 226 NaI(Tl) scintillation detectors surrounding MINOS and covering angles between 15° and 118° with respect to the target center. The response functions of DALI2<sup>+</sup> for  $\gamma$ -ray-source and in-beam measurements were simulated with the GEANT4 toolkit [39]. The relative agreement between the simulated and measured  $\gamma$ -ray-source efficiencies is within 5%. The reaction fragments were analyzed by the large acceptance 2.7-T SAMURAI spectrometer. The fragment-particle identification was done by trajectory reconstruction using two multiwire drift chambers placed upstream and downstream of SAMURAI for the magnetic rigidity information, while the TOF and  $\Delta E$  were provided by a 24 plastic scintillator-bar hodoscope for the fragment velocity and atomic number ( $Z$ ) determination. A particle identification with  $4.8$  ( $7.2$ ) $\sigma$  separation in  $Z$  and  $31$  ( $8.1$ ) $\sigma$  separation in  $A/Q$  was achieved for the beam (fragmentlike) Ca isotopes. The  $^{52}\text{Ca}$  beam particles had a kinetic energy at the reaction

vertex between 190 and 270 MeV/nucleon with a mid-target energy of  $\sim 230$  MeV/nucleon. The  $(p, pn)$  reaction channel was tagged by gating on  $^{52}\text{Ca}$  in BigRIPS, a high-momentum-transfer proton in MINOS, and  $^{51}\text{Ca}$  in SAMURAI, in coincidence. A total of 37 000 such events were recorded. The detection efficiency of MINOS for  $^{52}\text{Ca}(p, pn)^{51}\text{Ca}$  was 65(3)%, obtained from experimental data as in [38]. Two plastic scintillator arrays, the NeuLAND [40] demonstrator and NEBULA [41], were placed after the SAMURAI magnet for neutron detection. The kinematics of the high-momentum transfer  $(p, pn)$  quasifree scattering reaction leads to neutrons recoiling at large scattering angles mainly outside the neutron detectors' acceptance. On the other hand, events of proton inelastic scattering followed by neutron evaporation,  $^{52}\text{Ca}(p, p')^{52}\text{Ca}^* \rightarrow ^{51}\text{Ca} + n$ , [ $S_n(^{52}\text{Ca}) = 6.005(1)$  MeV [42]] could be detected. These events were subtracted after efficiency correction to extract quasifree scattering cross sections. The efficiency correction was applied as a function of the relative energy of  $(^{51}\text{Ca} + n)$  leading to a mean neutron detection efficiency of 32(4)%.

The Doppler-shift corrected  $\gamma$ -ray spectrum obtained from the deexcitation of the  $^{51}\text{Ca}$  reaction residues is shown in Fig. 1. In order to improve the full-energy-peak efficiency, an add-back analysis was performed for hits in detectors located within 12 cm from each other and a  $\gamma$ -particle time window was imposed for increasing the peak-to-total ratio.  $\gamma$ -ray transitions were found at the following energies: 3453(20) keV, 2375(13) keV, 1720(25) keV, 1461(20) keV, and 691(4) keV, with the significance levels of over  $5\sigma$ ,  $3\sigma$ ,  $2.5\sigma$ ,  $3\sigma$ , and  $3\sigma$ , respectively. These energies are in agreement with those found in the literature [43,44]. The level scheme of  $^{51}\text{Ca}$ , consistently obtained from this work and previous studies [43,44], is shown in the inset of Fig. 1. The simulated resolution for a 3.4-MeV  $\gamma$  ray emitted by particles with  $\beta = 0.6$  was 9% (FWHM) with a photopeak efficiency of 19%. The extracted inelastic scattering leading to bound  $^{51}\text{Ca}$  residues,  $^{52}\text{Ca}(p, p')^{52}\text{Ca}^* \rightarrow ^{51}\text{Ca} + n$  (neutron evaporation), corresponds to a cross section of 5.1(2) mb, 8.4% of the total events, predominantly in the population of the states leading to the 1720-keV, 2375-keV, and 1461-keV transitions. The associated  $(p, pn)$  cross sections after subtracting the neutron-evaporation contribution are 30.3(42) mb for populating the ground state, 22.3(24) mb (3453-keV state), 0.6(3) mb (1720-keV state), 0.9(6) mb (3836-keV state), and 0.9(2) mb (4144-keV state). The strong population of the  $3/2^-$  ground state and  $7/2^-$  3453-keV state is consistent with the  $(p_{3/2})^3$  and  $(f_{7/2})^{-1}(p_{3/2})^4$  single-particle configurations, respectively. The direct population of the  $7/2_1^-$ ,  $3/2_1^-$ , and  $(1/2_1^-)$  states corresponds to the neutron knockout off the  $f_{7/2}$ ,  $p_{3/2}$ , and  $p_{1/2}$  orbitals as illustrated in Fig. 1. The cross sections are listed in Table I.

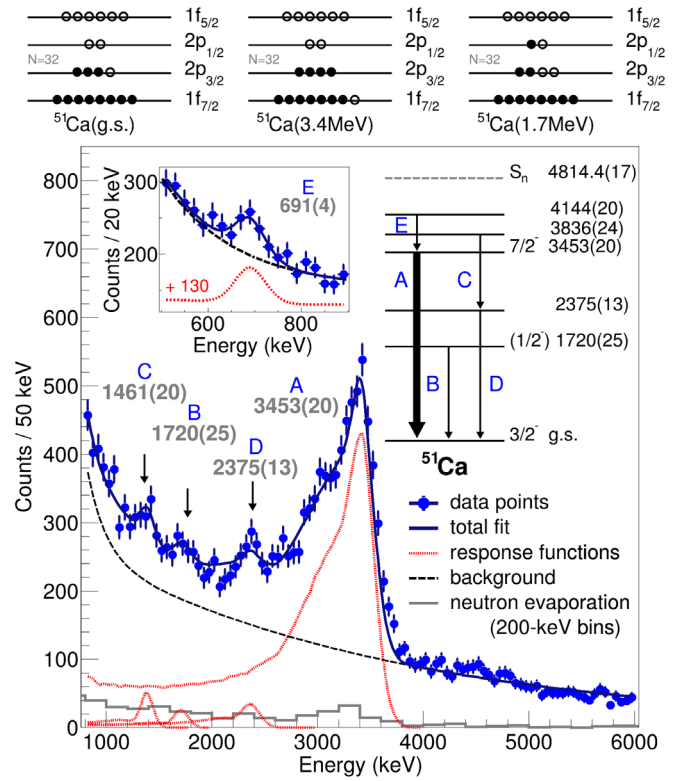


FIG. 1. Top: single-particle neutron configurations of  $^{51}\text{Ca}$  corresponding to the ground state, 3.4 MeV, and 1.7 MeV excited states, from left to right. Bottom: the  $\gamma$ -ray decay spectrum of  $^{51}\text{Ca}$  via the  $(p, pn)$  reaction after Doppler-shift and add-back correction (blue circles), including the neutron-evaporation contribution (gray line). The experimental  $\gamma$  spectrum is fitted (dark-blue line) with the simulated response functions (dotted red line) and a double-exponential background (dashed black line). The left-hand-side inset shows the low-energy region of the spectrum containing the transition at 691(4) keV, where the response function is shifted vertically (+130) for visualization. The level and decay scheme of  $^{51}\text{Ca}$  is summarized on the right.

The parallel and perpendicular momentum distributions (PMDs) of the  $^{51}\text{Ca}$  fragments relative to the beam were determined using the measured velocities and reconstructed angles at the reaction vertex. The differential PMDs  $d\sigma/dP_{\parallel}$  and  $d\sigma/dP_{\perp}$  to individual final states were constructed gating on each bin of the inclusive momentum and fitting the corresponding partial  $\gamma$ -ray spectra the same way as described for the total  $\gamma$ -ray spectrum. In this way the PMDs for the  $7/2^-$  state were obtained, while the ground-state PMDs are the difference between the total and the excited-state PMDs. The other non-ground-state components were found negligible. The neutron-evaporation events were subtracted from all PMDs. The experimental PMDs are shown in Fig. 2.

The theoretical momentum distributions were calculated within the distorted-wave impulse approximation (DWIA) formalism [45–49]. The folding potential (FP) [50] with the Melbourne  $G$ -matrix interaction [51] was used for



TABLE I. Experimental excitation energies ( $E_{\text{ex}}^{\text{exp}}$ ) with associated spin-parity assignment ( $J^\pi$ ) and the experimental cross sections ( $\sigma_{-1n}^{\text{th}}$ ) using  $r_0 = 1.21(5)$  fm,  $1.35(10)$  fm, and  $1.27$  fm (default) for the neutron knockout from  $f_{7/2}$ ,  $p_{3/2}$ , and  $p_{1/2}$  orbitals, respectively, together with the SM prediction for the excitation energies of  $^{51}\text{Ca}$  ( $E_{\text{ex}}^{\text{SM}}$ ) and  $\text{C}^2\text{S}_{\text{SM}}$ . The theoretical cross sections  $\sigma_{-1n}^{\text{th}}$  are calculated using the shell model  $\text{C}^2\text{S}_{\text{SM}}$  and the DWIA single-particle cross section values,  $\sigma_{\text{sp}}^{\text{DWIA}}$ . The ratio of experimental and theoretical single-particle cross sections normalized to  $(2J+1)$  is given in the last column.

$E_{\text{ex}}^{\text{exp}}$ (keV)	$J^\pi$	$-1n$	$\sigma_{-1n}^{\text{exp}}$ (mb)	$E_{\text{ex}}^{\text{SM}}$ (keV)	$\text{C}^2\text{S}_{\text{SM}}$	$\sigma_{\text{sp}}^{\text{DWIA}}$ (mb)	$\sigma_{-1n}^{\text{th}}$ (mb)	$\sigma_{-1n}^{\text{exp}}/(2J+1)\sigma_{\text{sp}}^{\text{DWIA}}$
0	$3/2^-$	$p_{3/2}$	30.3(42)	0	3.7	6.5(9)	23.9(32)	1.17(23)
1720(25)	$(1/2^-)$	$p_{1/2}$	0.6(3)	1.620	0.1	4.8	0.5	0.06(3)
3453(20)	$7/2^-$	$f_{7/2}$	22.3(24)	3.927	7.4	3.4(4)	25.0(27)	0.83(12)

incoming and outgoing nucleon scattering waves. The single-particle wave function of the knocked-out neutron was obtained as a bound state in the Bohr-Mottelson potential [52]. The Woods-Saxon one-body potential was used with the radial extension  $r_0 = 1.27$  fm and diffuseness  $a_0 = 0.67$  fm parameters as a starting point, and with the depth of the potential adjusted to match the neutron effective separation energy throughout the study [53]. The nonlocality correction was made to both the scattering and bound-state wave functions by using the Perey factor [54]. The elementary  $p$ - $n$  scattering process was described by the

nucleon-nucleon effective interaction parametrized by Franey and Love [55]; the Möller factor [56] was introduced for treating the Lorentz transformation of the  $p$ - $n$  cross section. The theoretical shapes were folded with the reaction energy profile and the experimental momentum resolution. The momentum profile of the direct  $^{52}\text{Ca}$  beam contained the main information on the experimental momentum resolution of  $49.5$  MeV/ $c$  ( $76.5$  MeV/ $c$ ) for the parallel (perpendicular) component to which an additional degradation of the resolution of  $1.5$  MeV/ $c$  ( $7.5$  MeV/ $c$ ) originating from the vertex position uncertainty inside the target is considered. The momentum profile of the direct  $^{52}\text{Ca}$  beam and the theoretical distributions for  $^{51}\text{Ca}$ , for populating the ground state and the 3453-keV excited state by  $p_{3/2}$  and  $f_{7/2}$  neutron knockout, respectively, are also plotted in Fig. 2.

For the  $(p, pn)$  reaction at  $\sim 230$  MeV/nucleon incident energy, the quasifree scattering approximation is proven to be suitable from the observed kinematics. The PMDs relate to the single-particle wave functions of the knocked-out neutrons, and therefore to their rms radii [57]. We conducted a variation of  $r_0$  and  $a_0$  of the Woods-Saxon potential used for the calculation of the wave function of the knocked-out neutron. It was found that the PMDs are not sensitive to  $a_0$ ; a change of  $a_0$  by 10% (40%), causes a PMDs width variation by less than 1% (4%). Calculations with the Dirac phenomenology potential EDAD1 (Dirac) [58] were also performed to estimate the impact of the choice of potential on the PMDs; in this case, the nonlocality correction to the scattering waves was made by multiplying them by the Darwin factor [46,59] in the Dirac phenomenology. The folding and Dirac potentials lead to almost identical PMDs within 4.5% for all considered  $(r_0, a_0)$  combinations (Fig. 2) and therefore the choice of potential has no significant impact on the PMDs and rms radii study. The momentum distributions and single-particle cross sections were calculated with FP for a range of  $r_0$  values keeping  $a_0 = 0.67$  fm. A  $\chi^2$  criterion was used and a probability analysis assuming a Gaussian probability density function was performed in order to determine the rms radii of the individual orbitals within our framework. Figures 2(c) and 2(d), show the reduced  $\chi^2$  distribution and

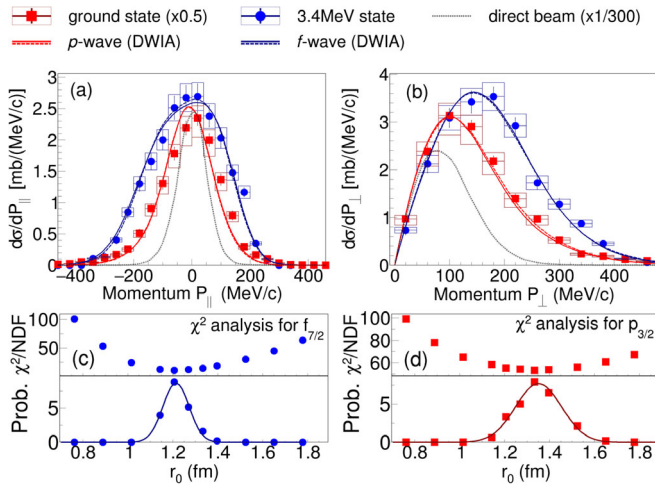


FIG. 2. Experimental parallel (a) and perpendicular (b) momentum distributions of the  $^{52}\text{Ca}$  direct beam (dotted black line),  $^{51}\text{Ca}$  ground-state (red squares), and 3453-keV state (blue circles) population together with the theoretical curves for  $p$ -wave (red) and  $f$ -wave (blue), with a binning of  $40$  MeV/ $c$ . The calculations were performed using a folding potential (solid lines) and the Dirac phenomenology potential (dashed lines) with  $a_0 = 0.67$  fm and the optimal  $r_0$  values:  $1.35$  fm ( $p$  wave) and  $1.21$  fm ( $f$  wave). The statistical errors are marked with crosses and the systematic errors on the absolute normalization with boxes. The (c) and (d) panels show the reduced  $\chi^2$  (upper panels), i.e.,  $\chi^2/\text{NDF}$  (NDF being the number of degrees of freedom), and the probability distribution (lower panels) for the  $f_{7/2}$  and  $p_{3/2}$  orbitals as a function of the parameter  $r_0$ . Study performed for vertex kinetic energies between  $190$  and  $270$  MeV/nucleon. See text for details.

the corresponding probability distribution as function of  $r_0$ . The optimal  $r_0$  and associated 1- $\sigma$  uncertainty for neutron knockout from the  $p_{3/2}$  and  $f_{7/2}$  orbitals are 1.35(10) fm and 1.21(5) fm, respectively. The deduced  $r_0$  values correspond to the rms radii of the single-particle wave functions of the knocked-out neutron of 4.74(18) fm for  $p_{3/2}$  and 4.13(14) fm for  $f_{7/2}$ . The single-particle wave functions were also obtained from Hartree-Fock-Bogolyubov (HFB) calculations using the HFBRAD [60] code and the SKM Skyrme interaction [61]. The SKM interaction was chosen for its best agreement to experimental data for the proton and matter radii. The rms radii of the single-particle wave function in this case were found at 4.49 fm for the  $p_{3/2}$  orbital and 4.12 fm for the  $f_{7/2}$  orbital, the rms radius of  $f_{7/2}$  being in perfect agreement with the rms radius obtained with the optimal  $r_0$ , while the  $p_{3/2}$  radius is underestimated. The proton, neutron, and matter total density rms radii obtained with HFB calculations with the SKM interaction for  $^{52}\text{Ca}$  are 3.46 fm, 3.74 fm, and 3.63 fm. Experimental data from isotopic shift measurements situate the charge distribution radius at 3.55 fm [25] and thus the proton rms radius at 3.46 fm [32]. The “unexpectedly” large charge radius for  $^{52}\text{Ca}$  found by [25] is explained by [31] proposing a “pronounced halo nature” of the  $p_{3/2}$  and  $p_{1/2}$  orbitals, 0.7 fm larger than the rms radii of the  $f_{5/2}$  and  $f_{7/2}$  orbitals. The rms radii difference between the  $p_{3/2}$  orbital and the  $f_{7/2}$  orbital obtained by the present analysis is 0.61(23) fm, in agreement with this prediction.

The calculated single-particle cross sections with  $r_0 = 1.27$  fm are 5.8 mb ( $p_{3/2}$ ), 3.8 mb ( $f_{7/2}$ ), and 4.8 mb ( $p_{1/2}$ ). Using the optimum  $r_0$  values obtained in this work, 6.5(9) mb and 3.4(4) mb were found for  $p_{3/2}$  and  $f_{7/2}$  orbitals, respectively. The single-particle cross sections are listed in Table I. Shell-model (SM) calculations were carried out with the pf-shell part of the PFSDG-U [62] interaction assuming a  $^{40}\text{Ca}$  core and a neutron effective charge of  $0.46e$ . The calculations predict the following occupation numbers for  $^{52}\text{Ca}$ : 7.803 ( $f_{7/2}$ ), 3.857 ( $p_{3/2}$ ), 0.142 ( $p_{1/2}$ ), and 0.198 ( $f_{5/2}$ ), corresponding to a neutron shell closure at  $N = 32$ . In comparison, the following occupation numbers are obtained for  $^{48}\text{Ca}$  and  $^{54}\text{Ca}$ : 7.704 and 7.809 ( $f_{7/2}$ ), 0.171 and 3.944 ( $p_{3/2}$ ), 0.023 and 1.861 ( $p_{1/2}$ ), and 0.103 and 0.064 ( $f_{5/2}$ ). The resulting excitation energies and spectroscopic factors to  $^{51}\text{Ca}$  are gathered in Table I.

The occupancies can be tested using neutron knockout cross sections and we use the ratio between the experimental and the single-particle cross sections normalized to  $(2J + 1)$ ,  $R_S = \sigma_{-1n}/(2J + 1)\sigma_{\text{sp}}$  in comparing  $^{52}\text{Ca}$  relative to  $^{48}\text{Ca}$  and  $^{54}\text{Ca}$ , considered as doubly closed-shell neutron-rich Ca isotopes [21–24,63]. For the systematic comparison, the theoretical single-particle cross sections obtained with the best-fit  $r_0$  values are used for  $^{52}\text{Ca}$ . The

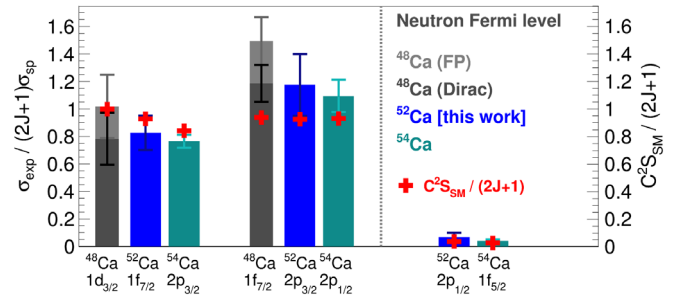


FIG. 3. The ratio of experimental neutron knockout cross sections and theoretical single-particle cross sections normalized to  $(2J + 1)$  for  $^{48,52,54}\text{Ca}$  (gray, blue, and turquoise, respectively) below and above the corresponding shell closures. Experimental data are from [24,64] and this work. The error bars contain experimental cross-section uncertainties. For  $^{52}\text{Ca}$ , theoretical uncertainties from the  $r_0$  sensitivity study are added quadratically.

$^{48}\text{Ca}(p, pn)$  triple-differential cross section (TDX) was studied at 149.5 MeV/nucleon by [64]. The theoretical single-particle TDX for the  $^{48}\text{Ca}(p, pn)$  reaction was calculated both with the FP, as for  $^{52}\text{Ca}$ , and Dirac. At higher reaction energies, as in the present experiment, the difference in cross sections between FP and Dirac are below 5%, but at  $\sim 150$  MeV/nucleon as for  $^{48}\text{Ca}$  from [64], the differences become significant. Dirac is more suitable for the stable  $^{48}\text{Ca}$ . The following values were obtained for the proportionality factors between the experimental and calculated TDX after the normalization to  $(2J + 1)$ , equivalent to  $R_S$ : 1.49(17) (FP) and 1.19(13) (Dirac) for the  $f_{7/2}$  orbital and 1.02(23) (FP) and 0.78(19) (Dirac) for the  $d_{3/2}$  orbital. The ratio between experimental and theoretical cross sections for  $^{54}\text{Ca}$  from [24], reporting on data obtained from the same measurement as the present work, is used for the comparison. The values for  $R_S$  for  $^{48}\text{Ca}$  (with FP and Dirac),  $^{52}\text{Ca}$ , and  $^{54}\text{Ca}$  for the orbitals below and above the neutron Fermi level are plotted in Fig. 3 together with the  $C^2 S_{\text{SM}}$ . The three Ca isotopes exhibit a consistent pattern: a ratio close to unity below the Fermi level and a very small ratio above. The  $N = 32$  shell closure in  $^{52}\text{Ca}$  thus proves to be as strong as  $N = 28$  and  $N = 34$  in Ca isotopes. This finding justifies the use of single-particle wave functions in this work.

To summarize, the  $(p, pn)$  one-neutron knockout from  $^{52}\text{Ca}$  at  $\sim 230$  MeV/nucleon was measured. Exclusive cross sections to bound final states in  $^{51}\text{Ca}$  and the momentum distributions corresponding to the removal of  $1f_{7/2}$  and  $2p_{3/2}$  neutrons were measured and analyzed within the DWIA framework. A consistent shell structure for  $^{48,52,54}\text{Ca}$  was obtained from the ratio of experimental and single-particle cross sections. The agreement with shell-model predictions places  $^{52}\text{Ca}$  among the doubly magic Ca isotopes. In addition, the measured momentum distributions with high statistics allowed to access the rms radii of

the  $1f_{7/2}$  and  $2p_{3/2}$  neutron orbitals at 4.13(14) fm and 4.74(18) fm, respectively. With this result, the  $p_{3/2}$  neutron single-particle orbital rms radius, 0.61(23) fm larger than  $1f_{7/2}$ , supports the prediction of [31] where the large spatial extension of  $p$  neutron orbitals in neutron-rich Ca isotopes is proposed to be responsible for the linear increase of their charge radii beyond  $^{48}\text{Ca}$ . The present result calls for a systematic extension of the method to several isotopic chains, complementary to ongoing efforts to explore the neutron radial extension in radioactive nuclei [65–69], relevant to the nuclear equation of state and the physics of neutron stars [70–73].

We are grateful for the support of the RIKEN Nishina Center accelerator staff in the delivery of the primary beam and the BigRIPS team for preparing the secondary beams. We thank Y. Chazono for the  $^{48}\text{Ca}(p, pn)$  knockout triple differential cross section calculations. M. E., H. N. L., A. O., T. A., I. G., C. L., D. R., H. T., V. W., and L. Z. acknowledge the support from the Deutsche Forschungsgemeinschaft (DFG, German Research Foundation), Project No. 279384907–SFB 1245. H. N. L. is supported by the Fundamental Research Funds for the Central Universities. K. O. acknowledges the support by Grants-in-Aid for Scientific Research from the JSPS (No. JP21H00125). A. P. is funded by Grant No. CEX2020-001007-S funded by MCIN/AEI/10.13039/501100011033 and PGC-2018-94583. Y. T. acknowledges the support from the JSPS Grant-in-Aid for Scientific Research Grants No. JP21H01114. B. D. L. and L. X. C. acknowledge support from the Vietnam Ministry of Science and Technology under Grant No. ĐTCB.01/21/VKHKHTN. D. S. acknowledges the National Research, Development and Innovation Fund of Hungary via project No. K128947. F. B. was supported by the RIKEN Special Postdoctoral Researcher Program. V. W. acknowledges the BMBF Grants No. 05P21RDFN1 and No. 05P21RDFN9. The development of M. I. N. O. S. has been supported by the European Research Council through the ERC Grant No. MINOS-258567.

\*mravar@ikp.tu-darmstadt.de

†hongna.liu@bnu.edu.cn

- [1] M. Mayer and J. H. D. Jensen, *Elementary Theory of Nuclear Shell Structure* (Wiley, New York, 1955).
- [2] T. Otsuka, A. Gade, O. Sorlin, T. Suzuki, and Y. Utsuno, *Rev. Mod. Phys.* **92**, 015002 (2020).
- [3] F. Nowacki, A. Poves, and A. Obertelli, *Prog. Part. Nucl. Phys.* **120**, 103866 (2021).
- [4] B. Bastin, S. Grevy, D. Sohler, O. Sorlin, Z. Dombradi, N. L. Achouri *et al.*, *Phys. Rev. Lett.* **99**, 022503 (2007).
- [5] A. Navin, D. W. Anthony, T. Aumann, T. Baumann, D. Bazin, Y. Blumenfeld *et al.*, *Phys. Rev. Lett.* **85**, 266 (2000).
- [6] C. Thibault, R. Klapisch, C. Rigaud, A. M. Poskanzer, R. Prieels, L. Lessard, and W. Reisdorf, *Phys. Rev. C* **12**, 644 (1975).
- [7] D. Guillemaud-Mueller, C. Detraz, M. Langevin, F. Naulin, M. de Saint-Simon, C. Thibault, F. Touchard, and M. Epherre, *Nucl. Phys.* **A426**, 37 (1984).
- [8] T. Motobayashi, Y. Ikedaa, Y. Ando, K. Ieki, M. Inoue, N. Iwasa *et al.*, *Phys. Lett. B* **346**, 9 (1995).
- [9] D. Steppenbeck, S. Takeuchi, N. Aoi, P. Doornenbal, M. Matsushita, H. Wang *et al.*, *Phys. Rev. Lett.* **114**, 252501 (2015).
- [10] A. Huck, G. Klotz, A. Knipper, C. Miehé, C. Richard-Serre, G. Walter, A. Poves, H. L. Ravn, and G. Marguier, *Phys. Rev. C* **31**, 2226 (1985).
- [11] R. Kanungo, I. Tanihata, A. Ozawa, *Phys. Lett. B* **528**, 58 (2002).
- [12] R. V. F. Janssens, B. Fornal, P. F. Mantica, B. A. Brown, R. Broda, P. Bhattacharyya *et al.*, *Phys. Lett. B* **546**, 55 (2002).
- [13] J. I. Prisciandaro, P. F. Mantica, B. A. Brown, D. W. Anthony, M. W. Cooper, A. Garcia *et al.*, *Phys. Lett. B* **510**, 17 (2001).
- [14] M. L. Cortés, W. Rodriguez, P. Doornenbal, A. Obertelli, J. D. Holt, J. Menéndez *et al.*, *Phys. Rev. C* **102**, 064320 (2020).
- [15] D.-C. Dinca, R. V. F. Janssens, A. Gade, D. Bazin, R. Broda, B. A. Brown *et al.*, *Phys. Rev. C* **71**, 041302(R) (2005).
- [16] A. Bürger, T. R. Saito, H. Grawe, H. Hübel, P. Reiter, J. Gerl *et al.*, *Phys. Lett. B* **622**, 29 (2005).
- [17] F. Wienholtz, D. Beck, K. Blaum, Ch. Borgmann, M. Breitenfeldt, R. B. Cakirli *et al.*, *Nature (London)* **498**, 346 (2013).
- [18] M. Rosenbusch, P. Ascher, D. Atanasov, C. Barbieri, D. Beck, K. Blaum *et al.*, *Phys. Rev. Lett.* **114**, 202501 (2015).
- [19] X. Xu, M. Wang, Y. Zhang, H. Xu, P. Shuai, X. Tu *et al.*, *Chin. Phys. C* **39**, 104001 (2015).
- [20] E. Leistenschneider, M. P. Reiter, S. Ayet San Andres, B. Kootte, J. D. Holt, P. Navratil *et al.*, *Phys. Rev. Lett.* **120**, 062503 (2018).
- [21] D. Steppenbeck, S. Takeuchi, N. Aoi, P. Doornenbal, M. Matsushita, H. Wang *et al.*, *Nature (London)* **502**, 207 (2013).
- [22] H. N. Liu, A. Obertelli, P. Doornenbal, C. A. Bertulani, G. Hagen, J. D. Holt *et al.*, *Phys. Rev. Lett.* **122**, 072502 (2019).
- [23] S. Michimasa, M. Kobayashi, Y. Kiyokawa, S. Ota, D. S. Ahn, H. Baba *et al.*, *Rev. Lett.* **121**, 022506 (2018).
- [24] S. Chen, J. Lee, P. Doornenbal, A. Obertelli, C. Barbieri, Y. Chazono *et al.*, *Phys. Rev. Lett.* **123**, 142501 (2019).
- [25] R. F. Garcia Ruiz, M. L. Bissell, K. Blaum, A. Ekström, N. Frömmgen, G. Hagen *et al.*, *Nat. Phys.* **12**, 594 (2016).
- [26] Á. Koszorús, X. F. Yang, W. G. Jiang, S. J. Novario, S. W. Bai, J. Billowes *et al.*, *Nat. Phys.* **17**, 439 (2021).
- [27] K. Kreim, M. L. Bissell, J. Papuga, K. Blaum, M. De Rydt, R. F. Garcia Ruiz *et al.*, *Phys. Lett. B* **731**, 97 (2014).
- [28] Y. L. Sun, A. Obertelli, P. Doornenbal, C. Barbieri, Y. Chazono, T. Duguet *et al.*, *Phys. Lett. B* **802**, 135215 (2020).
- [29] T. Koiwai, K. Wimmer, P. Doornenbal, A. Obertelli, C. Barbieri, T. Duguet *et al.*, *Phys. Lett. B* **827**, 136953 (2022).



- [30] F. Sommer, K. Konig, D. M. Rossi, N. Everett, D. Garand, R. P. deGroote *et al.*, *Phys. Rev. Lett.* **129**, 132501 (2022).
- [31] J. Bonnard, S. M. Lenzi, and A. P. Zuker, *Phys. Rev. Lett.* **116**, 212501 (2016).
- [32] M. Tanaka, M. Takechi, A. Homma, M. Fukuda, D. Nishimura, T. Suzuki *et al.*, *Phys. Rev. Lett.* **124**, 102501 (2020).
- [33] T. Kubo, D. Kameda, H. Suzuki, N. Fukuda, H. Takeda, Y. Yanagisawa *et al.*, *Prog. Theor. Exp. Phys.* **2012**, 03C003 (2012).
- [34] N. Fukuda, T. Kubo, T. Ohnishi, N. Inabe, H. Takeda, D. Kameda, and H. Suzuki, *Nucl. Instrum. Methods Phys. Res., Sect. B* **317**, 323 (2013).
- [35] T. Kobayashi *et al.*, *Nucl. Instrum. Methods Phys. Res., Sect. B* **317**, 294 (2013).
- [36] A. Obertelli, A. Delbart, S. Anvar, L. Audirac, G. Authelet, H. Baba *et al.*, *Eur. Phys. J. A* **50**, 8 (2014).
- [37] S. Takeuchi, T. Motobayashi, Y. Togano, M. Matsushita, N. Aoi, K. Demichi, H. Hasegawa, and H. Murakami, *Nucl. Instrum. Methods Phys. Res., Sect. A* **763**, 596 (2014).
- [38] C. Santamaria, A. Obertelli, S. Ota, M. Sasano, E. Takada, L. Audirac *et al.*, *Nucl. Instrum. Methods Phys. Res., Sect. A* **905**, 138 (2018).
- [39] S. Agostinelli, J. Allison, K. Amako, J. Apostolakis, H. Araujo, P. Arce *et al.*, *Nucl. Instrum. Methods Phys. Res., Sect. A* **506**, 250 (2003).
- [40] K. Boretzky, I. Gašparić, M. Heil, J. Mayer, A. Heinz, C. Caesar *et al.*, *Nucl. Instrum. Methods Phys. Res., Sect. A* **1014**, 165701 (2021).
- [41] T. Nakamura and Y. Kondo, *Nucl. Instrum. Methods Phys. Res., Sect. B* **376**, 156 (2016).
- [42] M. Wang, W. J. Huang, F. G. Kondev, G. Audi, S. Naimi, *Chin. Phys. C* **45**, 030003 (2021).
- [43] M. Rejmund, S. Bhattacharyya, A. Navin, W. Mittig, L. Gaudefroy, M. Gelin, G. Mukherjee, F. Rejmund, P. Roussel-Chomaz, and Ch. Theisen, *Phys. Rev. C* **76**, 021304(R) (2007).
- [44] B. Fornal, R. V. F. Janssens, R. Broda, N. Marginean, S. Beghini, L. Corradi *et al.*, *Phys. Rev. C* **77**, 014304 (2008).
- [45] N. S. Chant and P. G. Roos, *Phys. Rev. C* **15**, 57 (1977).
- [46] T. Wakasa, K. Ogata, and T. Noro, *Prog. Part. Nucl. Phys.* **96**, 32 (2017).
- [47] G. Jacob and Th. A. J. Maris, *Rev. Mod. Phys.* **38**, 121 (1966).
- [48] G. Jacob and Th. A. J. Maris, *Rev. Mod. Phys.* **45**, 6 (1973).
- [49] P. Kitching, W. J. McDonald, Th. A. J. Maris, and C. A. Z. Vasconcellos, *Adv. Nucl. Phys.* **15**, 43 (1985).
- [50] M. Toyokawa, K. Minomo, and M. Yahiro, *Phys. Rev. C* **88**, 054602 (2013).
- [51] K. Amos, P. J. Dortmans, H. V. von Geramb, S. Karataglidis and J. Raynnal, *Adv. Nucl. Phys.* **25**, 276 (2000).
- [52] A. Bohr and B. R. Mottelson, *Nuclear Structure: Single-Particle Motion and Nuclear Deformations* (World Scientific, Singapore, 1969), Vol. 1.
- [53] K. Yoshida, *Few-Body Syst.* **62**, 28 (2021).
- [54] F. G. Perey, *Direct Interactions and Nuclear Reaction Mechanism* (Gordon and Breach Science Publishers, New York, 1963), p. 125.
- [55] M. A. Franey and W. G. Love, *Phys. Rev. C* **31**, 488 (1985).
- [56] C. Möller, C. Barbieri, D. Bazin, C. A. Bertulani, A. Bonaccorso, W. H. Dickhoff *et al.*, *Kgl. Danske Videnskab. Selsbak, Mat-fys. Medd.* **23**, 1 (1945).
- [57] T. Aumann *et al.*, *Prog. Part. Nucl. Phys.* **118**, 103847 (2021).
- [58] E. D. Cooper, S. Hama, B. C. Clark, and R. L. Mercer, *Phys. Rev. C* **47**, 297 (1993).
- [59] L. G. Arnold, B. C. Clark, R. L. Mercer, and P. Schwandt, *Phys. Rev. C* **23**, 1949 (1981).
- [60] K. Bennaceur and J. Dobaczewski, *Comput. Phys. Commun.* **168**, 96 (2005).
- [61] J. Bartel, P. Quentin, M. Brack, C. Guet, H.-B. Hakansson, *Nucl. Phys.* **A386**, 79 (1982).
- [62] F. Nowacki, A. Poves, E. Caurier, and B. Bounthong, *Phys. Rev. Lett.* **117**, 272501 (2016).
- [63] F. Browne, S. Chen, P. Doornenbal, A. Obertelli, K. Ogata, Y. Utsuno *et al.*, *Phys. Rev. Lett.* **126**, 252501 (2021).
- [64] M. Ahmad, J. W. Watson, D. W. Devins, B. S. Flanders, D. L. Friesel, N. S. Chant, P. O. Roos, and J. Wastell, *Nucl. Phys.* **A424**, 92 (1984).
- [65] V. Lapoux, V. Somà, C. Barbieri, H. Hergert, J. D. Holt, and S. R. Stroberg, *Phys. Rev. Lett.* **117**, 052501 (2016).
- [66] P. Egelhof, S. Bagchi, S. Bönig, M. Csatlós, I. Dillmann, C. Dimopoulou *et al.*, *J. Phys. Soc. Jpn. Conf. Proc.* **6**, 020049 (2015).
- [67] K. Tsukada, A. Enokizono, T. Ohnishi, K. Adachi, T. Fujita, M. Hara *et al.*, *Phys. Rev. Lett.* **118**, 262501 (2017).
- [68] T. Aumann, C. A. Bertulani, F. Schindler, and S. Typel, *Phys. Rev. Lett.* **119**, 262501 (2017).
- [69] T. Aumann, W. Bartmann, O. Boine-Frankenheim, A. Bouvard, A. Broche, F. Butin *et al.*, *Eur. Phys. J. A* **58**, 88 (2022).
- [70] M. H. Mahzoon, M. C. Atkinson, R. J. Charity, and W. H. Dickhoff, *Phys. Rev. Lett.* **119**, 222503 (2017).
- [71] D. Adhikari *et al.* (PREX collaboration), *Phys. Rev. Lett.* **126**, 172502 (2021).
- [72] B. T. Reed, F. J. Fattoyev, C. J. Horowitz, and J. Piekarewicz, *Phys. Rev. Lett.* **126**, 172503 (2021).
- [73] J. M. Lattimer, *Annu. Rev. Part. Nucl. Sci.* **71**, 433 (2021).